Available online at www.sciencedirect.com
SCIENCE DIRECT®
Microporous and Mesoporous Materials 62 (2003) 73–79
MICROPOROUS AND MESOPOROUS MATERIALS
www.elsevier.com/locate/micromeso

Preparation and characterization of H_1–e rhodium films

Philip N. Bartlett *, Jan Marwan

Department of Chemistry, University of Southampton, Southampton SO17 1BJ, UK

Received 9 January 2003; received in revised form 29 April 2003; accepted 29 April 2003

Abstract

Mesoposous films of rhodium were prepared by electrochemical deposition from rhodium (III) chloride dissolved in the H_1 lyotropic liquid crystalline phase of octaethyleneglycol monohexadecyl ether ($C_{16}EO_8$) or Brij® 56. Characterization of the electrochemically deposited films using SEM, TEM, small angle X-ray diffraction and cyclic voltammetry show that they are smooth, strongly adherent, with a high surface area (32 $m^2 g^{-1}$) and containing a regular hexagonal array of cylindrical pores with a pore centre to pore centre separation of around 6 nm. Preliminary studies show that the films can be used to carry out the electrochemical reduction of nitrate in basic solution.

Keywords: Rhodium; Mesoporous; Template; Electrodeposition; Lyotropic liquid crystal

1. Introduction

Mesoporous metals with regular nanoarchitectures were first synthesised in Southampton using chemical or electrochemical reduction of a metal salt dissolved in the aqueous component of a lyotropic liquid crystalline phase formed from a non-ionic surfactant [1,2]. In this method high concentrations of surfactant (typically between 30 and 60 wt.%) are used and the mesoporous structure of the final metal is directly templated by the lyotropic liquid crystalline phase. Thus it is possible to produce mesoporous metals with different pore topologies and with different pore and wall thicknesses depending on the choice of surfactant and template solution composition [1].

Since the original studies on the electrochemical deposition of mesoporous platinum films [1,3–5] this approach has been extended to the deposition of several other metals including palladium [6], cobalt [7], nickel [8] and tin [9]. In this paper we describe the deposition of mesoporous rhodium films, their characterization using TEM, small angle X-ray diffraction and electrochemistry, and the results of a preliminary study of their use as catalysts for the electrochemical oxidation of nitrate. The rhodium films described are denoted as H_1–e films to indicate that they were electrochemically deposited from the H_1 hexagonal lyotropic liquid crystalline phase, in this case of octaethyleneglycol hexadecylether ($C_{16}EO_8$), and as a consequence contain a regular array of hexagonally packed pores.

* Corresponding author. Tel.: +44-2380-592373; fax: +44-2380-593781.
E-mail address: p.n.bartlett@soton.ac.uk (P.N. Bartlett).

1387-1811/03/$ - see front matter © 2003 Elsevier Inc. All rights reserved.
doi:10.1016/S1387-1811(03)00394-9

2. Experimental

Sulfuric acid (AnalaR BDH), sodium hydroxide (AnalaR BDH), sodium nitrate (Aldrich), rhodium (III) chloride (99.9% Alfa Aesar), octaethyleneglycol monohexadecyl ether ($C_{16}EO_8$, Fluka), Brij® 56 (Aldrich) and heptane (99%, Lancaster) were all used as received. All aqueous solutions were freshly prepared using reagent grade water (18 MΩ cm) from a Whatman "Stillplus" system coupled to a Whatman RO 50. All glassware was soaked overnight in a 3% Decon/deionised water solution and washed thoroughly at least 3 times with deionised water prior to use.

All electrochemical experiments were carried out using an EG&G Model 263A potentiostat/galvanostat with a large area platinum gauze counter electrode and a home made saturated calomel (SCE) or saturated mercury sulfate (SMSE) reference electrode (potentials with respect to SMSE are shifted 0.45 V negative of the corresponding potential vs. SCE). The reference electrode was used in conjunction with a luggin capillary and stored in a saturated potassium sulfate solution when not in use.

The H_1–e Rh films were freshly prepared before each electrochemical experiment by electrochemical deposition on to gold disc electrodes (area 0.0079 cm^2) formed by sealing 1 ± 0.1 mm diameter gold wire in glass, or onto gold microdisc electrodes (diameter 25 μm). Immediately before use the gold disc and microdisc electrodes were polished using alumina/water slurries (Beuhler) with particle sizes of 1.0 and then 0.3 μm. H_1–e Rh films were deposited from a solution containing 12 wt.% $RhCl_3$, 47 wt.% $C_{16}EO_8$ or Brij® 56, 39 wt.% water and 2 wt.% heptane at 25 °C. These conditions correspond to the hexagonal (H_1) lyotropic phase for the mixture as determined by studies of the phase diagram for the system (vide infra). The deposition mixture is highly viscous and must be prepared with care to ensure a uniform composition. After mixing all of the components the mixture was heated to around 60 °C and stirred by hand in order to ensure homogeneity and then cooled before use. The mixture was then checked using polarising light microscopy to ensure that it was in the hexagonal phase before use.

The phase behaviour of the pseudobinary mixtures was investigated by polarised light microscopy using an Olympus BH-2 polarised light microscope equipped with a Linkam TMS90 heating stage and temperature control unit. Phases were assigned on the basis of their characteristic optical textures [10]. The phase transition boundaries were located to an accuracy of ±2 °C by using heating/cooling rates of 0.2 °C min^{-1}.

Rhodium was deposited from the liquid crystalline plating mixture at −0.2 V vs. SCE. The total amount of the metal deposited, assuming 100% Faradaic efficiency for the process, was controlled by controlling the total amount of charge passed and was usually 0.44 C cm^{-2} corresponding to the deposition of 156 μg cm^{-2} of rhodium onto the electrodes. The deposition took typically 150 s. After deposition the H_1–e Rh films were soaked in water for at least 1 h to remove the surfactant.

Electrochemical measurements on the H_1–e Rh films were carried out at room temperature (18–23 °C) in 1 M H_2SO_4. Before each experiment the solution was sparged for 10–15 min with a stream of highly purified argon gas to displace dissolved oxygen. The electrochemically active surface areas of the films were estimated by integrating the charge passed in the surface oxide stripping reaction recorded in 1 M sulfuric acid following the procedure originally suggested by Rand and Woods [11].

SEM images were obtained using a JOEL 300 scanning electron microscope. Samples for SEM analysis were prepared by electroplating Rh from the template mixture on to evaporated gold electrodes (area 1 cm^2) prepared by evaporation of a 10 nm thick layer of chromium (to ensure good adhesion) followed by 200 nm of gold on 1 mm thick glass microscope slides. These evaporated gold electrodes were cleaned in an ultrasonic bath of 2-propanol for 10 min immediately before use. For transmission electron microscopy studies a JOEL 2000 TEM was used. The nanostructured Rh samples were strongly adherent on the gold electrode surface and samples for TEM analysis were prepared by scraping small samples of rhodium off of the evaporated gold electrode surface and on to the TEM grid using a scalpel. Small angle X-ray diffraction with Cu Kα radiation was

used to provide evidence for the formation of a regular nanostructured film.

3. Results

3.1. Phase behaviour

As demonstrated in our earlier work the nanoarchitecture of the final electrochemically deposited film is directly determined by the structure of the lyotropic phase used of deposition. We therefore begin by describing the phase behaviour of mixtures of the non-ionic surfactant ($C_{16}EO_8$) and the rhodium chloride solution, Fig. 1. The hexagonal, H_1, phase exists from 40 to 80 wt.% surfactant and at temperatures up to almost 50 °C at around 55 wt.%. The bicontinuous cubic, V_1, phase has a smaller region of existence between 50 and 80 wt.% surfactant and at higher temperatures. At higher surfactant concentrations the lamellar, L_α, phase predominates. The phase behaviour and location of the phase boundaries found for the rhodium chloride/$C_{16}EO_8$ systems are very similar to those reported by Mitchell [10] for the $C_{16}EO_8$ water system indicating that the presence of the rhodium salt does not significantly perturb the phase behaviour of the system. This contrasts with the findings for the corresponding platinum plating bath based on hexachloroplatinic acid where large shifts in the phase boundaries are observed [12] and have been attributed to strong interactions between the hexachloroplatinate anions and the ethylene oxide headgroups of the surfactant.

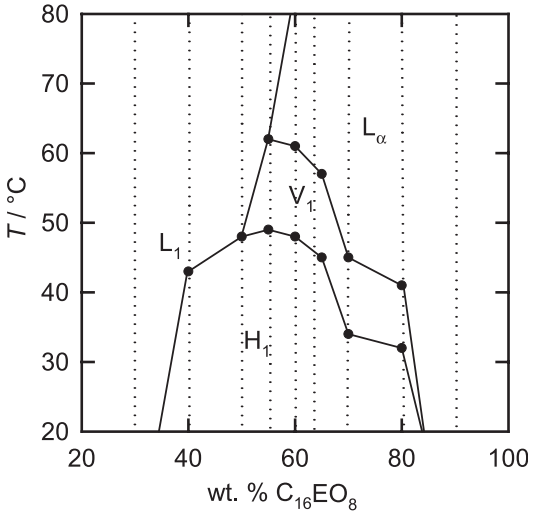

Fig. 1. Pseudobinary phase diagrams for $C_{16}EO_8$ and water in which the concentration of $RhCl_3$ was kept constant at 1.91 mol dm^{-3} and the ratio of surfactant to heptane was kept fixed at 22:1. The dotted lines show the compositions that were investigated. the solid lines which correspond to the domain boundaries are drawn as guides to the eye. H_1 is the hexagonal phase, V_1 the cubic phase, L_α the lamellar phase, and L_1 is the micellar solution.

The phase diagram in Fig. 1 shows a large composition and temperature range over which the hexagonal phase is stable. In all the subsequent experiments the H_1–e rhodium films were prepared by carrying out the deposition from this phase. Following deposition the surfactant was removed by soaking the film in water to leave a smooth adherent nanostructured rhodium film. Very similar mesoporous Rh films were also obtained by electrochemical deposition from plating mixtures in which the $C_{16}EO_8$ was replaced by Brij® 56 a commercial polydisperse surfactant mixture with a distribution of headgroup sizes, the major components (>5%) being from $C_{16}EO_4$ to $C_{16}EO_{12}$ with $C_{16}EO_8$ being the most abundant.

3.2. Characterization of H_1–e Rh films

The nanostructured rhodium films were characterized using SEM, TEM and small angle X-ray diffraction. Fig. 2 shows an SEM image of the fractured edge of the H_1–e rhodium film deposited on evaporated gold on glass. The film is smooth, uniform and dense, and clearly strongly adherent to the gold surface. Evidence for the nanostructure is provided by small angle X-ray diffraction, Fig. 3, which shows a well resolved peak at a value of 2θ corresponding to a lattice spacing of 4.9 nm corresponding to a pore centre to pore centre spacing of 5.6 nm. This is supported by transmission electron microscopy, Fig. 4 which clearly shows the regular hexagonal arrangement of uniform pores running through the metal. From the TEM we estimate that the pore centre to pore centre distance is 6.0 nm with a pore diameter of about 3.5 nm and a pore wall thickness of 2.5 nm. These values are very similar to those found for other nanoporous metals deposited under similar

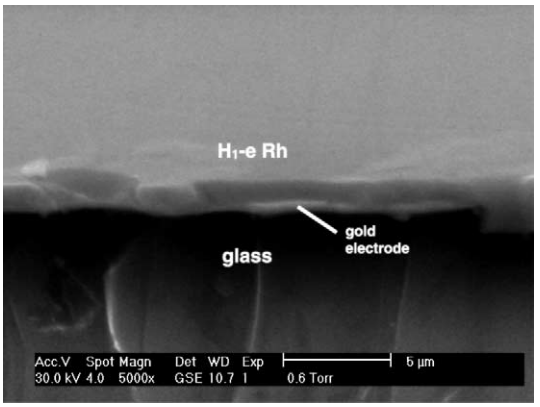

Fig. 2. Scanning electron micrograph of a fractured H_1–e Rh film deposited on an evaporated gold electrode. The image shows the film in cross-section with the glass support at the bottom, the protruding edge of the evaporated gold film and the rhodium film on the top. The film was deposited from a mixture of 12 wt.% $RhCl_3$, 47 wt.% $C_{16}EO_8$, 2 wt.% heptane and 39 wt.% water. The total charge passed was 0.56 C/cm^2 and the image was obtained at a tilt angle of 70°.

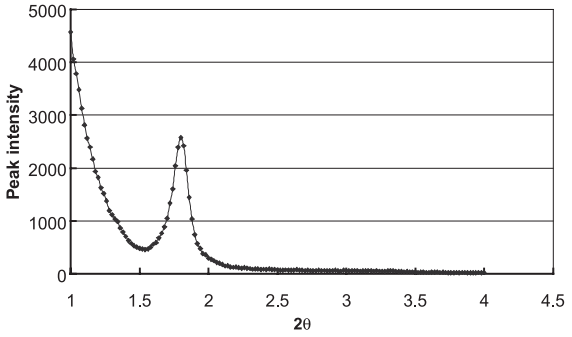

Fig. 3. Low angle X-ray diffraction of an H_1–e Rh film deposited on an evaporated gold electrode from a mixture of 12 wt.% $RhCl_3$, 47 wt.% $C_{16}EO_8$, 39 wt.% water and 2 wt.% heptane. The total charge passed for deposition was 0.70 C/cm^2.

conditions from the hexagonal lyotropic liquid crystalline phase formed by $C_{16}EO_8$ [1,6].

3.3. Electrochemistry of H_1–e Rh films

Fig. 5 shows a typical voltammogram recorded for an H_1–e rhodium film in 1 M sulfuric acid. The voltammetry of the nanostructured film is very similar to that reported in the literature for ordinary rhodium electrodes [13–16]. The formation of

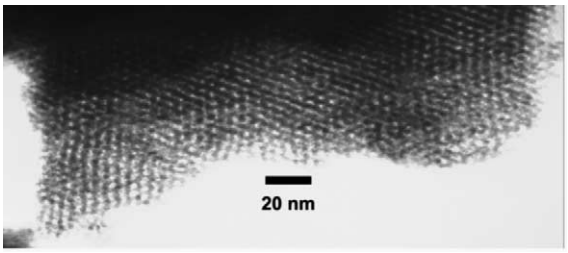

Fig. 4. Transmission electron micrograph of a sample of H_1–e Rh deposited from a mixture of 12 wt.% $RhCl_3$, 47 wt.% $C_{16}EO_8$, 2 wt.% heptane and 39 wt.% water.

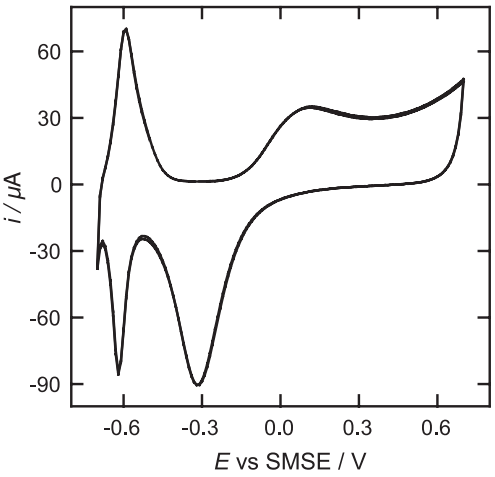

Fig. 5. Cyclic voltammogram of an H_1–e Rh film (126 nm thick, total deposition charge 3.5 mC) deposited from the $C_{16}EO_8$ template mixture on a gold disc electrode (area 0.0079 cm^2) recorded at 50 mV/s in 1 M sulfuric acid. The film was soaked in water for 1 h prior to the measurement.

a surface oxide film begins at around −0.16 V vs. SMSE on the anodic scan. This process leads first to the formation of Rh(OH) and then, at more anodic potentials to $Rh(OH)_3$ [14,16]. The existence of these surface oxides has been confirmed by XPS studies [17]. On the return, cathodic, sweep the surface oxide is removed in a single stripping peak which occurs, under our conditions, at −0.305 V vs. SMSE. The position of the oxide stripping peak for rhodium electrodes is known to be sensitive not only to the acid concentration but also to the anodic scan limit, the scan rate and number of scans [13,14,16]. For the H_1–e Rh films we find that the voltammetry for the oxide strip-

ping peak changes over the first ten or so cycles with the oxide stripping peak initially occurring at −0.53 V vs. SMSE but with this being replaced by the peak at −0.305 V seen in Fig. 5 over successive cycles. Throughout this process the total charge associated with the two peaks remains constant. Continuing the cathodic scan, the current at −0.62 V is associated with the formation of a layer of adsorbed hydrogen at the electrode surface which is then stripped from the surface on the anodic scan at −0.59 V. According to in situ infrared studies adsorbed hydrogen atoms on Rh exist in two distinguishable forms [18], however although at high acid concentration (>5 M) it is possible to distinguish these in the voltammetry in more dilute acidic solutions only the weakly bound adsorbed hydrogen is seen [15]. Again, as for the voltammetry at anodic potentials, the behaviour of the H_1–e rhodium film is identical to that for the ordinary rhodium electrode.

The voltammetry of the films in acid provides a very simple way in which to measure the electrochemically active surface area of the metal since we can use the charge associated with stripping of the oxide film to estimate the electrode area [14,19]. Using a conversion factor of 660 $\mu C/cm^2$ for the oxide stripping [14] we obtain a specific surface area for the H_1–e rhodium film of 32 $m^2\,g^{-1}$ which corresponds to an area per unit volume of 3.3×10^6 $cm^2\,cm^{-3}$ which is consistent with the nanostructure of the film found by TEM and X-ray. A very similar estimate of the surface area of the electrode (31 $m^2\,g^{-1}$) is obtained by integration of the charge associated with hydrogen adsorption at the electrode surface.

3.4. Electrochemical reduction of nitrate at the H_1–e rhodium surface

The electrochemical reduction of nitrate is of importance in the treatment of nuclear waste, in the cleanup of nitrate in the environment [20] and as the basis for the electrochemical detection of nitrate. The reduction of nitrate is a complex process involving a number of intermediate species both in solution and adsorbed at the electrode surface [21–24]. Studies of nitrate reduction on platinum, palladium and rhodium electrodes have shown that, of the three, rhodium is the most effective for nitrate reduction [20,21,25].

H_1–e metal film electrodes have a very high surface area contained in a small volume—typical specific surface areas for these films are of the order of 10^7 $cm^2\,cm^{-3}$. This can be a significant advantage in the case of electrode reactions where the rate is limited by a surface chemical reaction since the very high surface area can lead to an increase in the rate of this step relative to the rate of solution mass transport. This effect has already been demonstrated for H_1–e Pt electrodes for the reduction of oxygen [26] and for the oxidation and reduction of hydrogen peroxide [27]. In both cases the reactions involve chemical reactions (as distinct from electrochemical reactions where the rate is changed by increasing the overpotential) of surface bound species and at smooth Pt surfaces these can be rate limiting. By coating microelectrodes with high surface area nanostructured Pt films the analytical responses were significantly improved and mass transport limited currents were obtained indicating that the surface reactions were no longer rate limiting. In addition the electroanalytical responses of the electrodes were less susceptible to poisoning because the overall analytical signal was no longer controlled by the rate of the surface reaction.

In the present study we chose to investigate the use of an H_1–e Rh coated microelectrode for the electroreduction of nitrate in basic solution. Fig. 6 shows voltammograms for the H_1–e Rh microelectrode in 2 M NaOH both with and without nitrate in the solution. In the absence of nitrate the voltammogram is almost featureless except for a cathodic current peak around −1.25 V corresponding to the formation of adsorbed hydrogen on the electrode surface. Upon addition of nitrate to the solution there is a significant increase in the cathodic current which now increases to a maximum at around −1.28 V before falling sharply and on the return anodic scan the current crosses over the initial cathodic trace. This type of behaviour is indicative of a process which involves changes at the electrode surface and is very similar to that reported in the literature for nitrate reduction on plain Rh electrodes [21,25]. The standard potential for nitrate reduction in basic solution is around +0.01 V vs. SHE (corresponding to −0.68 V vs.

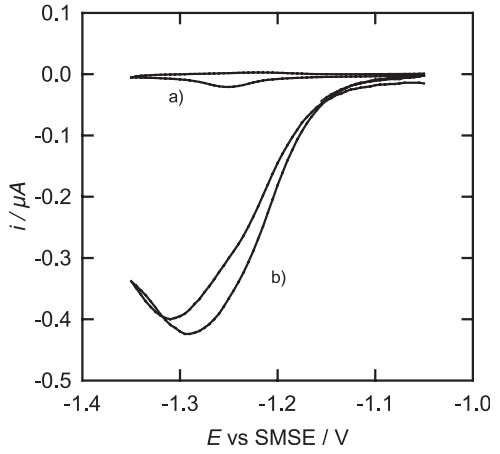

Fig. 6. Cyclic voltammograms for a H_1–e Rh coated 25 μm gold microelectrode (deposition charge 87 μC) recorded at 0.5 mV/s in 2 M NaOH (a) without and (b) with 30 mM $NaNO_3$ present.

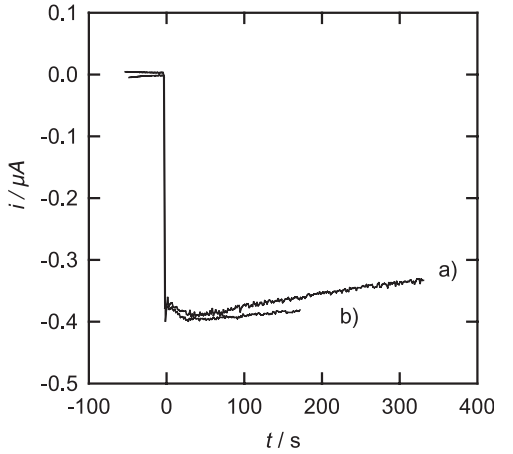

Fig. 7. Transient responses for an H_1–e Rh coated 25 μm diameter electrode following addition of 50 mM nitrate to 2 M NaOH recorded at −1.28 V vs. SMSE. The H_1–e Rh film was deposited onto the gold microelectrode surface from the template mixture using a deposition charge of 90 μC corresponding to a film thickness of 126 nm. Curves (a) and (b) show results for replicate measurements in fresh NaOH solution.

SMSE) significantly anodic of the current peak in the voltammetry [23]. From Fig. 6 it is also clear that the reduction of nitrate does not start on the Rh surface until adsorbed hydrogen is formed but that at high coverages of adsorbed hydrogen the reaction is inhibited. These observations suggest that the electroreduction of nitrate involves the reaction between an adsorbed nitrogen species at the electrode surface and adsorbed hydrogen but that the adsorbed hydrogen blocks adsorption of the nitrogen intermediate [21–23].

Fig. 7 shows the transient response of the microelectrode to the addition of nitrate to the solution. The current increases rapidly following addition of nitrate, as expected, but at longer times the current slowly decays. This effect is not due to irreversible poisoning of the Rh surface since when the experiment was repeated using the same electrode but transferred to a fresh NaOH solution the response to the addition of nitrate was almost identical (compare curves a and b in Fig. 7). These results suggest that the decrease in the response with time is due to the build up of some intermediate in the solution at the electrode surface which inhibits the reaction. A similar effect (not shown) was observed for a plain Rh coated microelectrode showing that this effect is not peculiar to the H_1–e Rh film.

Calibration curves for nitrate at the H_1–e coated Rh microelectrode were obtained by taking the initial currents following addition of nitrate, Fig. 8. These show a linear variation of the current with nitrate concentration up to at least 0.5 M

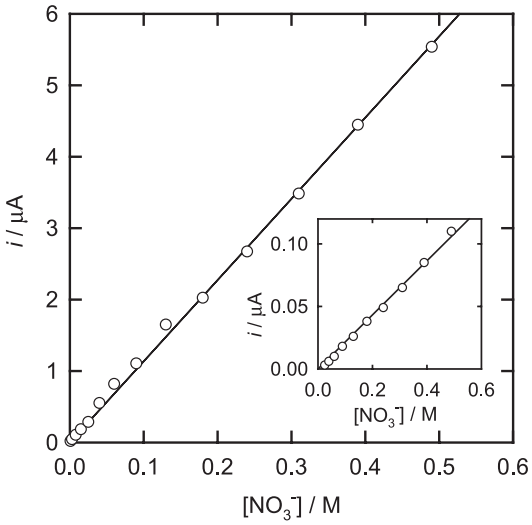

Fig. 8. Calibration curves for the reduction of nitrate at an H_1–e Rh coated 25 μm diameter gold microelectrode (deposition charge 90 μC) recorded −1.28 V vs. SMSE in 1 M NaOH. The inset shows the corresponding result for the same gold microdisc electrode coated with a plain Rh film deposited from an aqueous solution of $RhCl_3$ in 1 M HCl.

nitrate. When compared to the response of the plain Rh coated microelectrode (Fig. 8 inset) the currents at the H_1–e coated electrodes are significantly larger. The currents recorded for nitrate reduction are significantly less than those estimated for the mass transport limited 8 electron reduction of nitrate at the microelectrode (assuming a diffusion coefficient of 1.5×10^{-5} cm^2 s^{-1} [28]). This result, taken together with the fact that the increase in current at the nanostructured electrode scales with the surface area of the Rh, suggests that the current at the H_1–e Rh coated electrode is still determined by the rate of the surface reaction.

4. Conclusions

High surface area mesoporous rhodium films were synthesised by electrochemical deposition from the H_1 lyotropic liquid crystalline phase of octaethyleneglycol monohexadecyl ether ($C_{16}EO_8$). The resulting films are a direct cast of the template and contain a regular hexagonal array of cylindrical pores running through the electroplated rhodium films as demonstrated by transmission electron microscopy and small angle X-ray diffraction studies.

H_1–e Rh films deposited onto gold microelectrodes were used as electrodes for the reduction of nitrate in basic solution. The nitrate reduction currents were found to be significantly larger at the H_1–e Rh coated electrodes than at similar electrodes coated with plain Rh films indicating that the nitrate reduction current scales with the electroactive area under these conditions. Linear calibration curves up to 0.5 M nitrate were obtained.

Acknowledgements

J.M. thanks City Technology Ltd. for a postgraduate studentship. This work was supported in part by EPSRC grant GR/M51284.

References

[1] G.S. Attard, P.N. Bartlett, N.R.B. Coleman, J.M. Elliott, J.R. Owen, J.H. Wang, Science 278 (1997) 838.
[2] G.S. Attard, C.G. Göltner, J.M. Corker, S. Henke, R.H. Templer, Angew. Chem., Int. Ed. Engl. 36 (1997) 1315.
[3] J.M. Elliott, G.S. Attard, P.N. Bartlett, N.R.B. Coleman, D.A.S. Merckel, J.R. Owen, Chem. Mater. 11 (1999) 3602.
[4] J.M. Elliott, P.R. Birkin, P.N. Bartlett, G.S. Attard, Langmuir 15 (1999) 7411.
[5] J.M. Elliott, J.R. Owen, Phys. Chem. Chem. Phys. 2 (2000) 5653.
[6] P.N. Bartlett, B. Gollas, S. Guerin, J. Marwan, Phys. Chem. Chem. Phys. 4 (2002) 3835.
[7] P.N. Bartlett, P.R. Birkin, M.A. Ghanem, P. de Groot, M. Sawicki, J. Electrochem. Soc. 148 (2001) C119.
[8] P.A. Nelson, J.M. Elliott, G.S. Attard, J.R. Owen, Chem. Mater 14 (2002) 524.
[9] A.H. Whitehead, J.M. Elliott, J.R. Owen, G.S. Attard, Chem. Comm. (1999) 331.
[10] D.J. Mitchell, G.J.T. Tiddy, J. Waring, T. Bostock, M.P. McDonald, J. Chem. Soc., Faraday Trans. I 79 (1983) 975.
[11] D.A.J. Rand, R. Woods, J. Electroanal. Chem. 31 (1971) 29.
[12] G.S. Attard, P.N. Bartlett, N.R.B. Coleman, J.M. Elliott, J.R. Owen, Langmuir 14 (1998) 7340.
[13] C. Pallotta, N.R. De Tacconi, A.J. Arvia, Electrochim. Acta 26 (1981) 261.
[14] G. Jerkiewicz, J.J. Borodzinski, Langmuir 9 (1993) 2202.
[15] A. Capon, R. Parsons, J. Electroanal. Chem. 39 (1972) 275.
[16] F. Villiard, G. Jerkiewicz, Can. J. Chem. 75 (1997) 1656.
[17] M. Peuckert, Surf. Sci. 141 (1984) 500.
[18] A. Bewick, J.W. Russell, J. Electroanal. Chem. 142 (1982) 337.
[19] D.A.J. Rand, R. Woods, J. Electroanal. Chem. 31 (1970) 29.
[20] K.J. Reddy, J. Lin, Water Res. 34 (2000) 995.
[21] O.A. Petrii, T.Y. Safonova, J. Electroanal. Chem. 331 (1992) 897.
[22] M. Wasberg, G. Horanyi, Electrochim. Acta 40 (1995) 613.
[23] T. Ohmori, M.S. El-Deab, M. Osawa, J. Electroanal. Chem. 470 (1999) 46.
[24] M.C.P.M. da Cunha, J.P.I. De Souza, F.C. Nart, Langmuir 16 (2000) 771.
[25] G. Horanyi, M. Wasberg, Electrochim. Acta 42 (1997) 261.
[26] P.R. Birkin, J.M. Elliott, Y.E. Watson, J. Chem. Soc., Chem. Commun. (2000) 1693.
[27] S.A.G. Evans, J.M. Elliott, L.M. Andrews, P.N. Bartlett, P.J. Doyle, G. Deunault, Anal. Chem. 74 (2002) 1322.
[28] D.R. Lide, Handbook of Physics and Chemistry, 73rd ed., Elsevier, New York, 1992.